Graphene-Edge-Supported Iron Dual-Atom for Oxygen Reduction Electrocatalyst

Joel F. Sumbowo,[ab] Farhan A. Ihsan,[ab] Fadjar Fathurrahman,[bc] Nadya Amalia,[a] Fiki T. Akbar, [d], Hadi T. Yudistira,[e] Nadhratun N. Mobarak,[f] Hermawan K. Dipojono,[bc] Sasfan A. Wella,*[ag] and Adhitya G. Saputro*[bc]

[a] *Research Center for Quantum Physics, National Research and Innovation Agency (BRIN), South Tangerang 15314, Indonesia.*
[b] *Advanced Functional Materials Research Group, Faculty of Industrial Technology, Institut Teknologi Bandung, Bandung 40132, Indonesia.*
[c] *Research Center for Nanosciences and Nanotechnology, Institut Teknologi Bandung, Bandung 40132, Indonesia.*
[d] *Theoretical High Energy Physics Research Division, Faculty of Mathematics and Natural Sciences, Institut Teknologi Bandung, Bandung 40132, Indonesia.*
[e] *Mechanical Engineering Study Program, Institut Teknologi Sumatera (ITERA), South Lampung 35365, Indonesia.*
[f] *Department of Chemical Sciences, Faculty of Science and Technology, Universiti Kebangsaan Malaysia, Bangi 43600, Malaysia*
[g] *Collaboration Research Center for Advanced Energy Materials, Bandung 40132, Indonesia.*

*corresponding authors:
Sasfan A. Wella (sasfan.arman.wella@brin.go.id) and Adhitya G. Saputro (gandaryus@itb.ac.id)

1 Temperature and pressure dependence on formation energy

In order to gain a comprehensive understanding of the stability of Fe-DACs under various conditions, we also calculate the nitrogen chemical potential at specific temperatures and pressures using the following formula:

$$\begin{aligned}\mu_{\mathrm{N}}(T,P) &= \frac{1}{2}\left[\mu^{0}_{\mathrm{N_2}} + k_{\mathrm{B}}T\ln\left(\frac{P_{\mathrm{N_2}}}{P^{0}_{\mathrm{N_2}}}\right)\right] \\ &= \frac{1}{2}\left[E^{\mathrm{DFT}}_{\mathrm{N_2}} + \mathrm{ZPE}_{\mathrm{N_2}} - TS^{0}_{\mathrm{N_2}} + k_{\mathrm{B}}T\ln\left(\frac{P_{\mathrm{N_2}}}{P^{0}_{\mathrm{N_2}}}\right)\right],\end{aligned}$$

where, $E^{\mathrm{DFT}}_{\mathrm{N_2}}$ represents the total electronic energy obtained through density functional theory (DFT) calculations, $\mathrm{ZPE}_{\mathrm{N_2}}$ denotes the zero-point energy obtained from quantum mechanical calculations, $S^{0}_{\mathrm{N_2}}$ represents the entropy value at standard conditions acquired from experimental data, k_{B} is the Boltzmann constant, T is the temperature, and $P_{\mathrm{N_2}}$ is the pressure of nitrogen gas. In Fig. **??**, we illustrate the formation energy's dependency on $\Delta\mu_{\mathrm{N}}$, the difference between the nitrogen chemical potential at specific temperature T and pressure P and that at standard conditions (T =298 K and P=1 bar). $\Delta\mu_{\mathrm{N}}$=0 corresponds to μ_{N} from $\mathrm{N_2}$ under standard conditions, while $\Delta\mu_{\mathrm{N}}$=0.54 eV represents μ_{N} from graphitic carbon nitride (g$-\mathrm{C_3N_4}$).

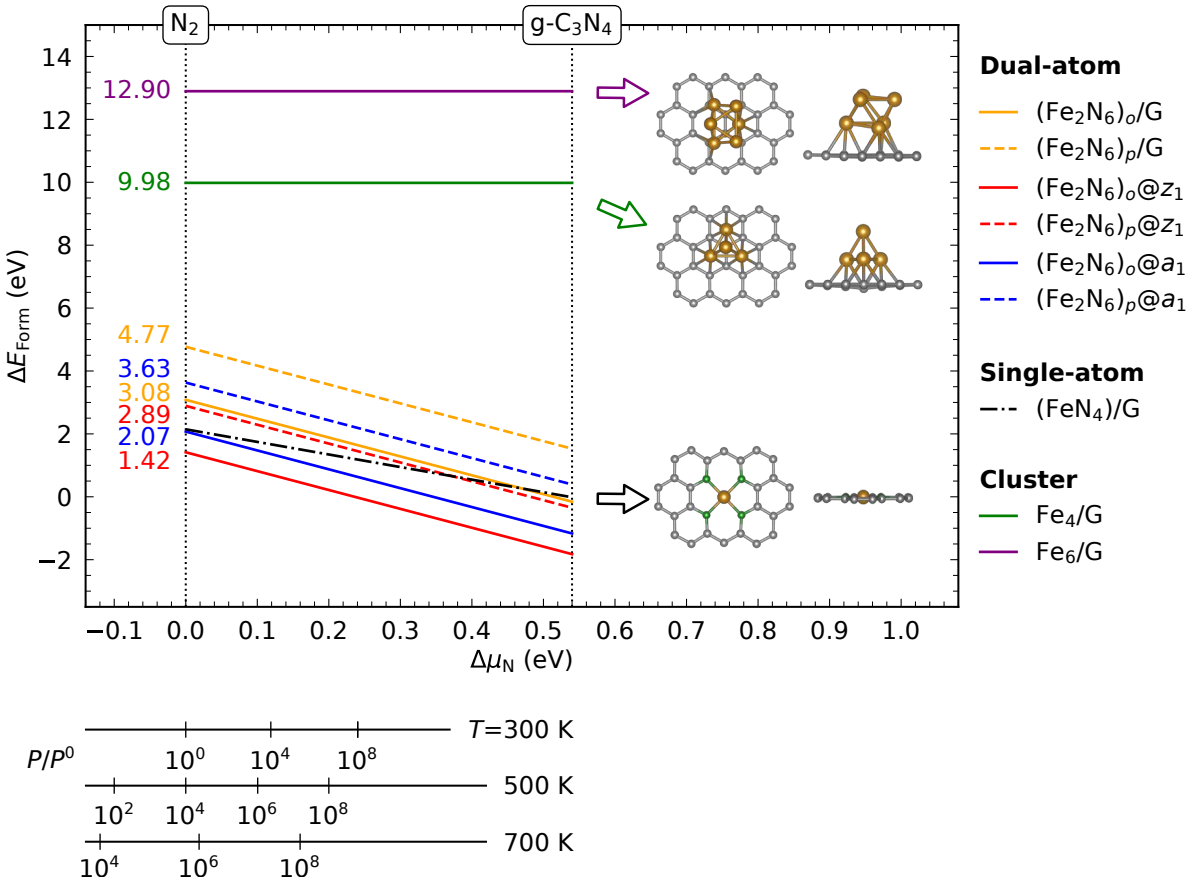

Figure S1: Relative formation energy of Fe_2N_6 active sites as a function of $\Delta\mu_N$, the difference between the nitrogen chemical potential at specific temperature T and pressure P and that at standard conditions (T =298 K and P =1 bar). The bottom axes show the corresponding N_2 chemical potentials at specific T and P.

2 Nitrogen effects on the stability of Fe-DACs

To confirm the importance of nitrogen in the stability of Fe-DAC structures, we also computed the formation energy of Fe-DAC in the absence of nitrogen atoms (denoted as Fe_2). We then compared the result with the formation energy of Fe_2N_6 at standard conditions, where the nitrogen chemical potential is calculated at $T = 298$ K and $P = 1$ bar. Significantly, as shown in Fig. **??**, the formation energy of Fe_2 is much higher than that of Fe_2N_6 across all configurations, confirming the crucial role of nitrogen atoms in stabilizing the Fe-DAC structures.

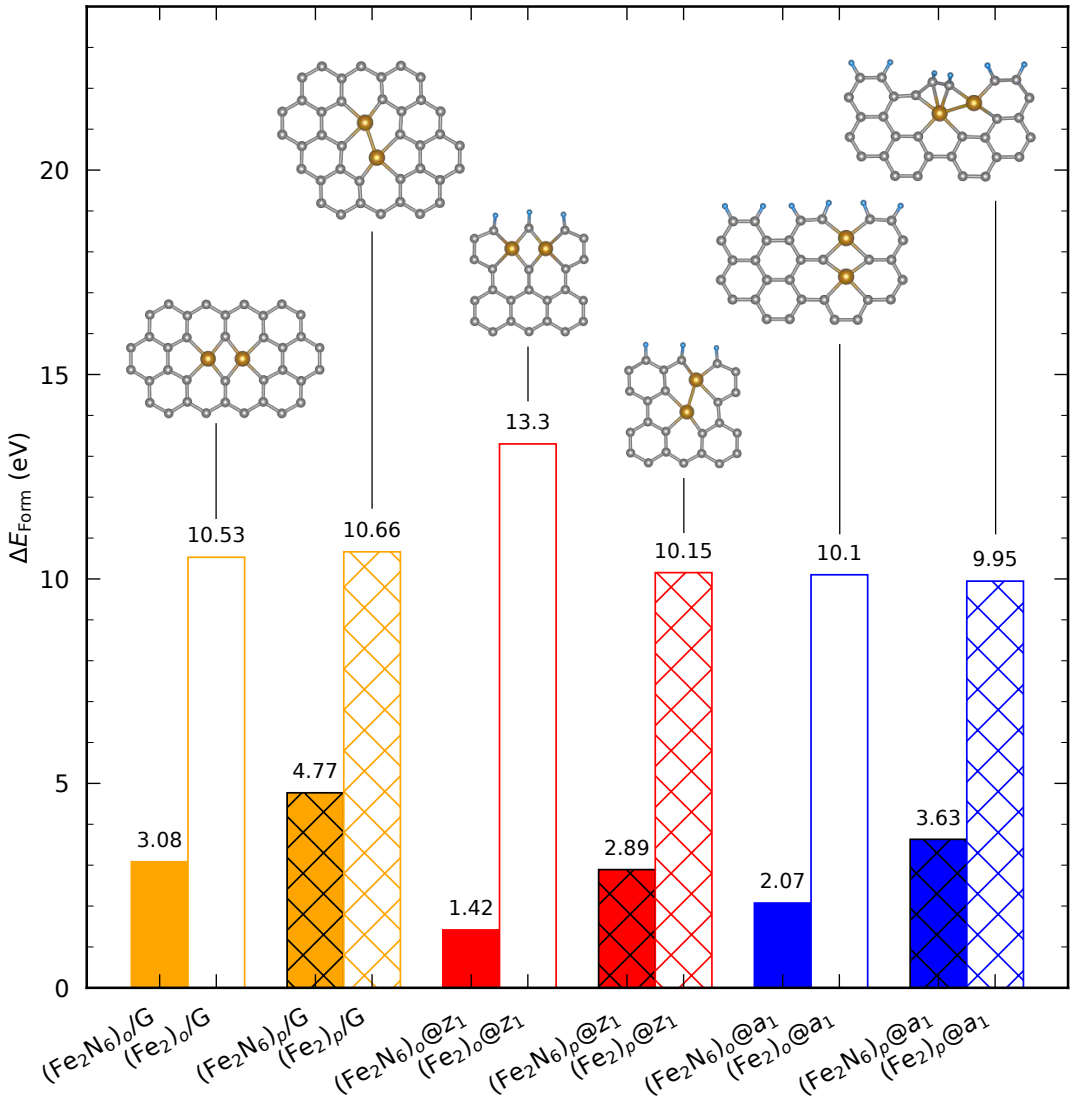

Figure S2: Formation energies of Fe-DACs with and without nitrogen.

3 Molecular adsorption energies on FeDAC active sites

Table S1: Adsorption energies of intermediate molecules (O_2, OOH, O, 2 OH, and OH) on each active site. The adsorption energies is defined as $E^{\text{ads}} = E_{\text{surf+adsorbate}} - (E_{\text{surf}} + E_{\text{ads}})$, where $E_{\text{surf+adsorbate}}$, E_{surf}, and $E_{\text{adsorbate}}$ represent the total energy (obtained from DFT calculations) of the clean surface, the adsorbed system, and the adsorbate in gaseous phase, respectively. Here, it is assumed that the adsorbed OOH is derived from O_2 molecule and one-half of H_2 molecule; adsorbed OH is derived from one-half of an H_2 molecule and one-half of an O_2 molecule; and 2 OH is determined by combining O_2 and H_2 molecules.

Active Sites	E^{ads} [eV]				
	$^*O_2$	*OOH	*O	*2 OH	*OH
Pt(111)	−1.04	−2.08	−0.12	−4.20	−1.96
$(Fe_2N_6)_o$/G	−0.94	−1.36	−0.40	−3.87	−1.73
$(Fe_2N_6)_p$/G	−1.97	−4.79	−2.44	−5.44	−3.12
$(Fe_2N_6)_o@z_1$	−0.77	−2.73	−0.53	−3.88	−2.02
$(Fe_2N_6)_p@z_1$	−2.17	−5.06	−2.76	−5.52	−3.22
$(Fe_2N_6)_o@a_1$	−0.97	−1.38	−0.60	−3.91	−1.60
$(Fe_2N_6)_p@a_1$	−2.20	−5.41	−2.81	−6.00	−3.33
$(Fe_2N_6)_p$-OH/G	−0.89	−2.84	−0.83	−4.33	−2.25
$(Fe_2N_6)_p$-OH$@z_1$	−0.97	−1.58	−1.07	−4.28	−2.33
$(Fe_2N_6)_p$-OH$@a_1$	−1.39	−3.53	−1.51	−4.90	−2.66

4 Rate determining step (RDS)

Table S2: The rate determining step (RDS) of the ORR with associative and dissociative mechanisms via both pathways A and B. RDS is determined by using surface coverage analysis.

Active sites	Rate Determining Step (RDS)			
	Associative		Dissociative	
	A	B	A	B
Pt(111)	(6)	(8b)	-	-
$(Fe_2N_6)_o$/G	(6)	(6)	(11)	(11)
$(Fe_2N_6)_p$/G	(9)	(9)	(15)	(15)
$(Fe_2N_6)_o$@z_1	(7a)	(7b)	(13a)	(13b)
$(Fe_2N_6)_p$@z_1	(9)	(9)	(15)	(15)
$(Fe_2N_6)_o$@a_1	(6)	(6)	(11)	(11)
$(Fe_2N_6)_p$@a_1	(9)	(9)	(15)	(15)
$(Fe_2N_6)_p$-OH/G	(8a)	(7b)	-	-
$(Fe_2N_6)_p$-OH@z_1	(6)	(6)	-	-
$(Fe_2N_6)_p$-OH@a_1	(9)	(9)	-	-

5 Fe-DACs in para configuration

(a) $(Fe_2N_6)_p$-OH/G

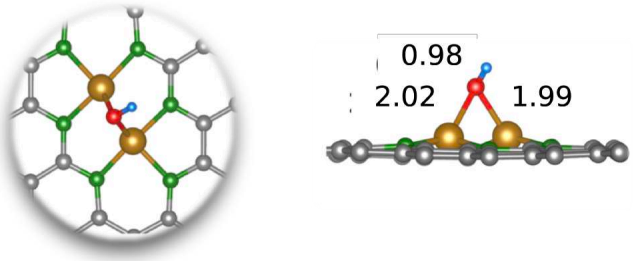

(b) $(Fe_2N_6)_p$-OH@z_1

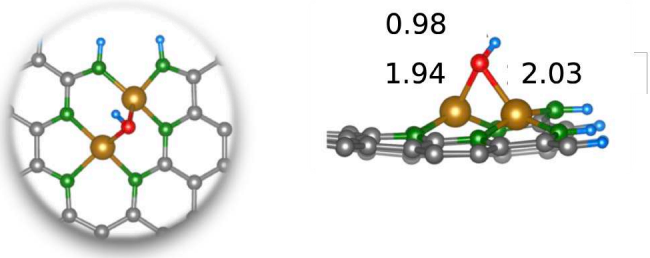

(b) $(Fe_2N_6)_p$-OH@a_1

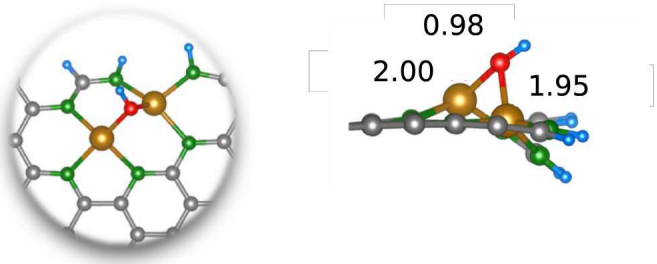

Figure S3: Optimized structure of Fe-DACs in *para* configuration, i.e. (a) $(Fe_2N_6)_p$-OH/G, (b) $(Fe_2N_6)_p$-OH@z_1 , and (c) $(Fe_2N_6)_p$-OH@a_1 , after OH poisoning. Grey, gold, red, green, and cyan spheres represent the C, Fe, O, N, and H atoms, respectively. Bond length is given in Å.

6 Oxygen dissociation mechanism

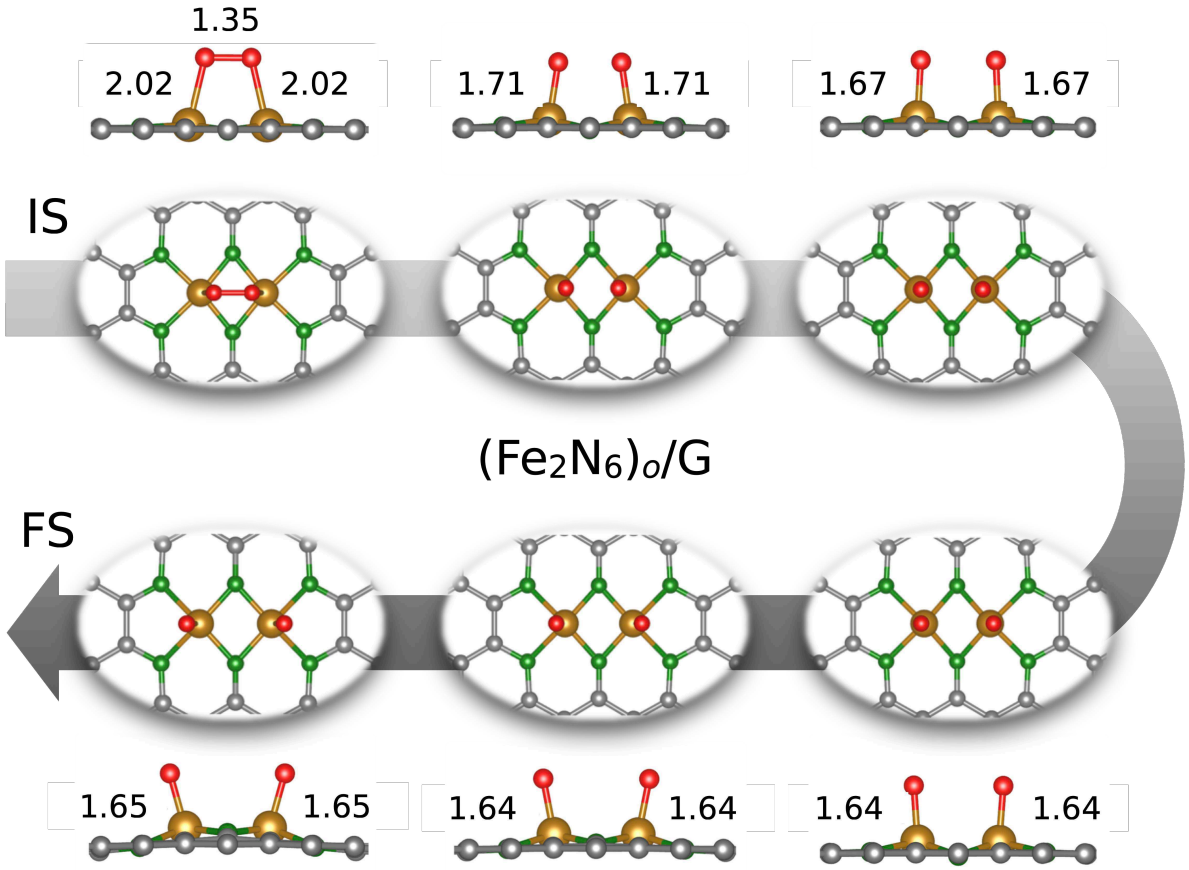

Figure S4: The O_2 dissociation on $(Fe_2N_6)_o$/G calculated using NEB method. Grey, gold, red, green, and cyan spheres represent the C, Fe, O, N, and H atoms, respectively. Bond length is given in Å. IS and FS indicate the initial and final states, respectively.

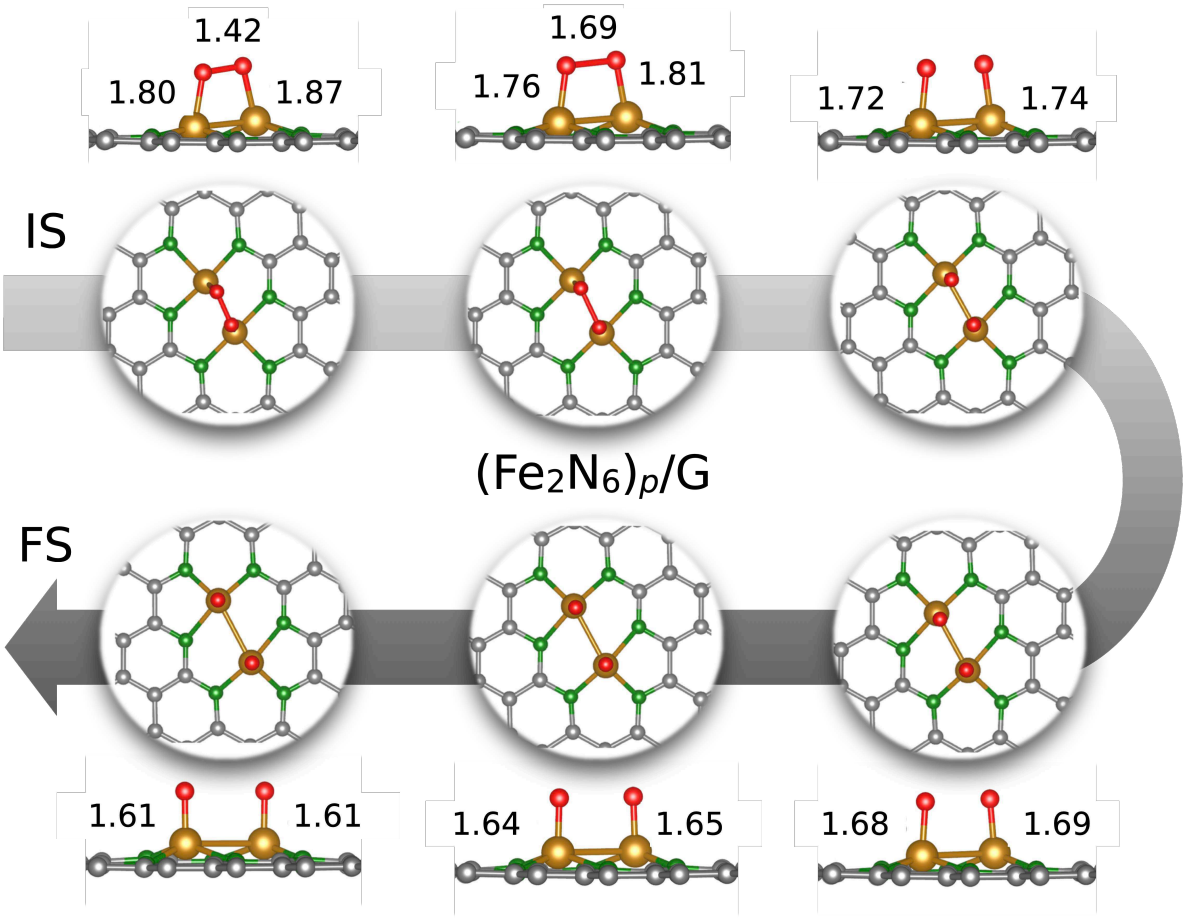

Figure S5: The O_2 dissociation on $(Fe_2N_6)_p$/G calculated using NEB method. Grey, gold, red, green, and cyan spheres represent the C, Fe, O, N, and H atoms, respectively. Bond length is given in Å. IS and FS indicate the initial and final states, respectively.

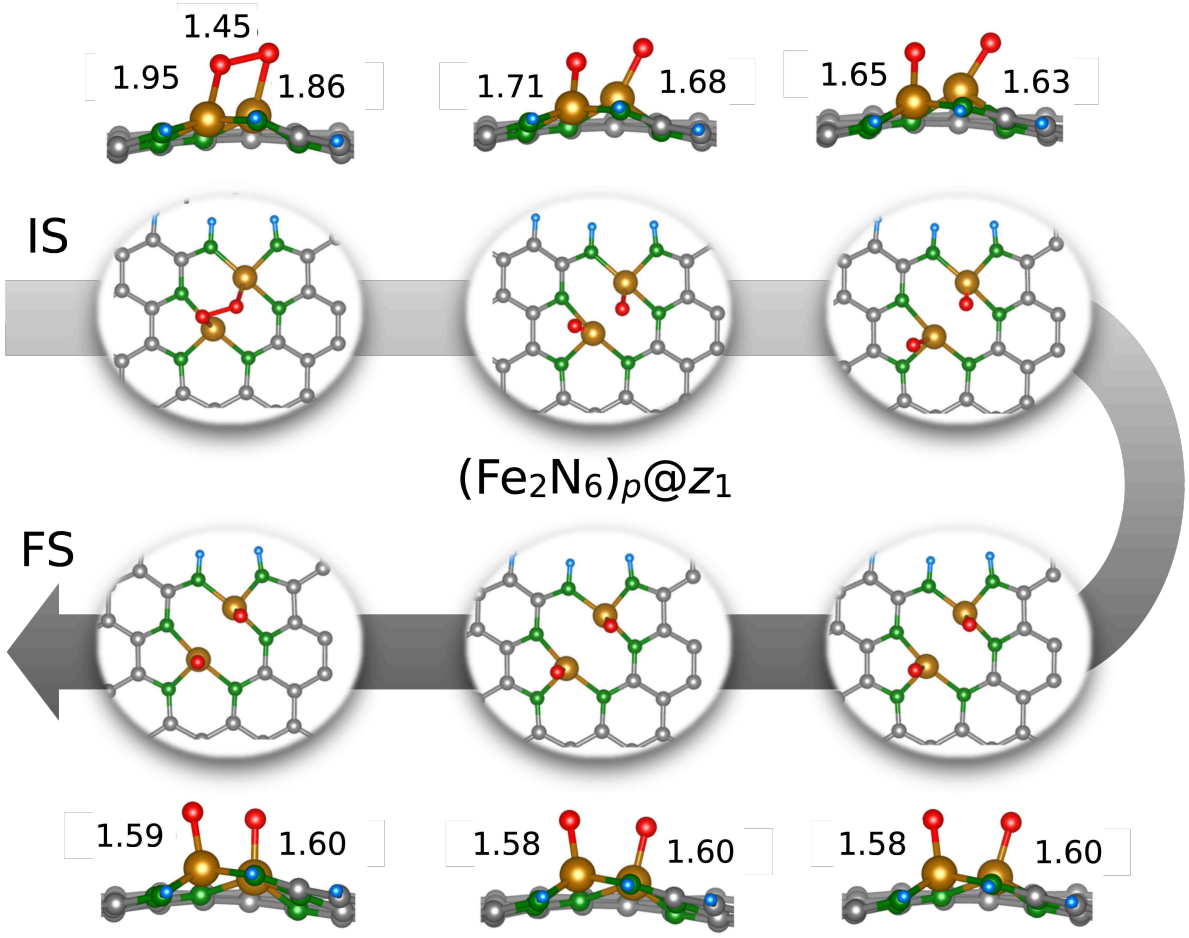

Figure S6: The O_2 dissociation on $(Fe_2N_6)_o@z_1$ calculated using NEB method. Grey, gold, red, green, and cyan spheres represent the C, Fe, O, N, and H atoms, respectively. Bond length is given in Å. IS and FS indicate the initial and final states, respectively.

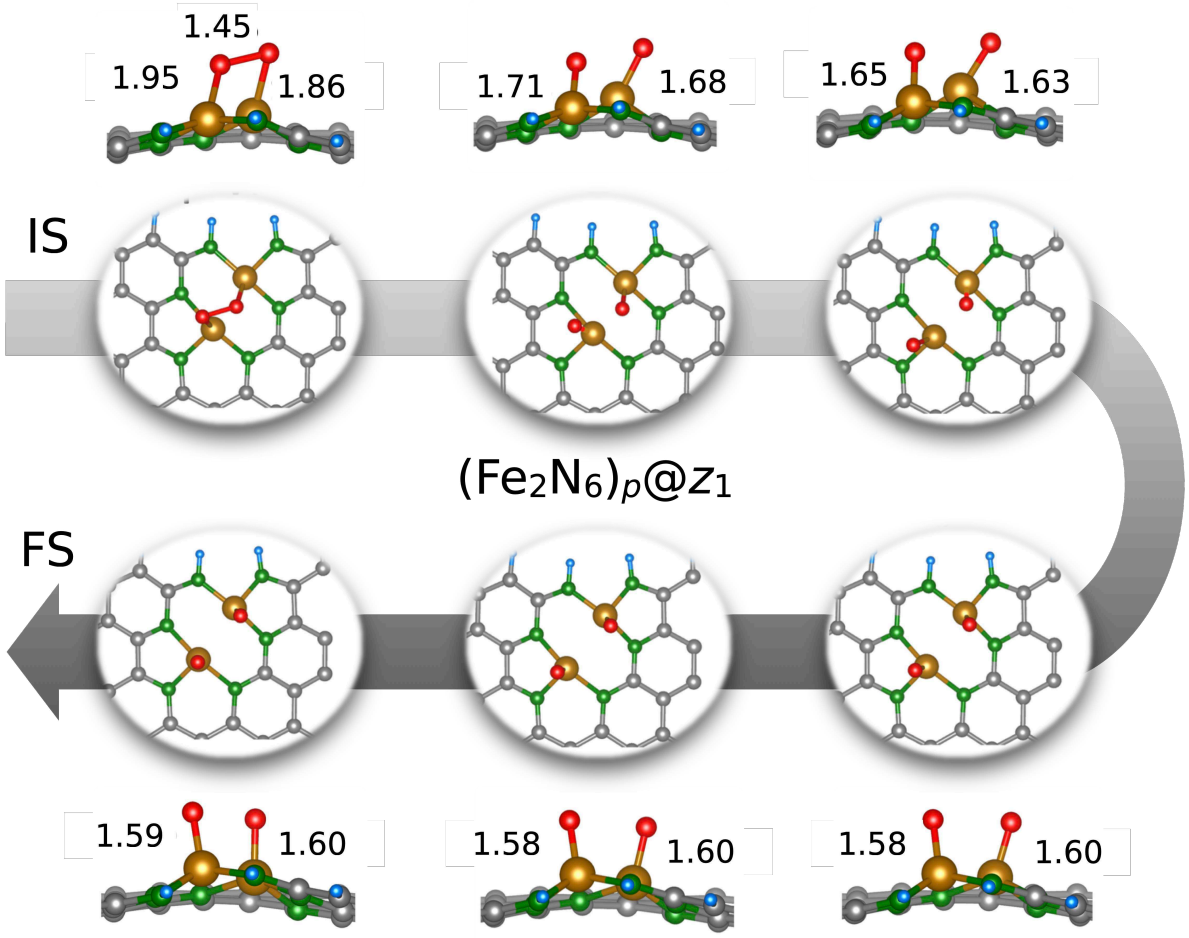

Figure S7: The O_2 dissociation on $(Fe_2N_6)_p@z_1$ calculated using NEB method. Grey, gold, red, green, and cyan spheres represent the C, Fe, O, N, and H atoms, respectively. Bond length is given in Å. IS and FS indicate the initial and final states, respectively.

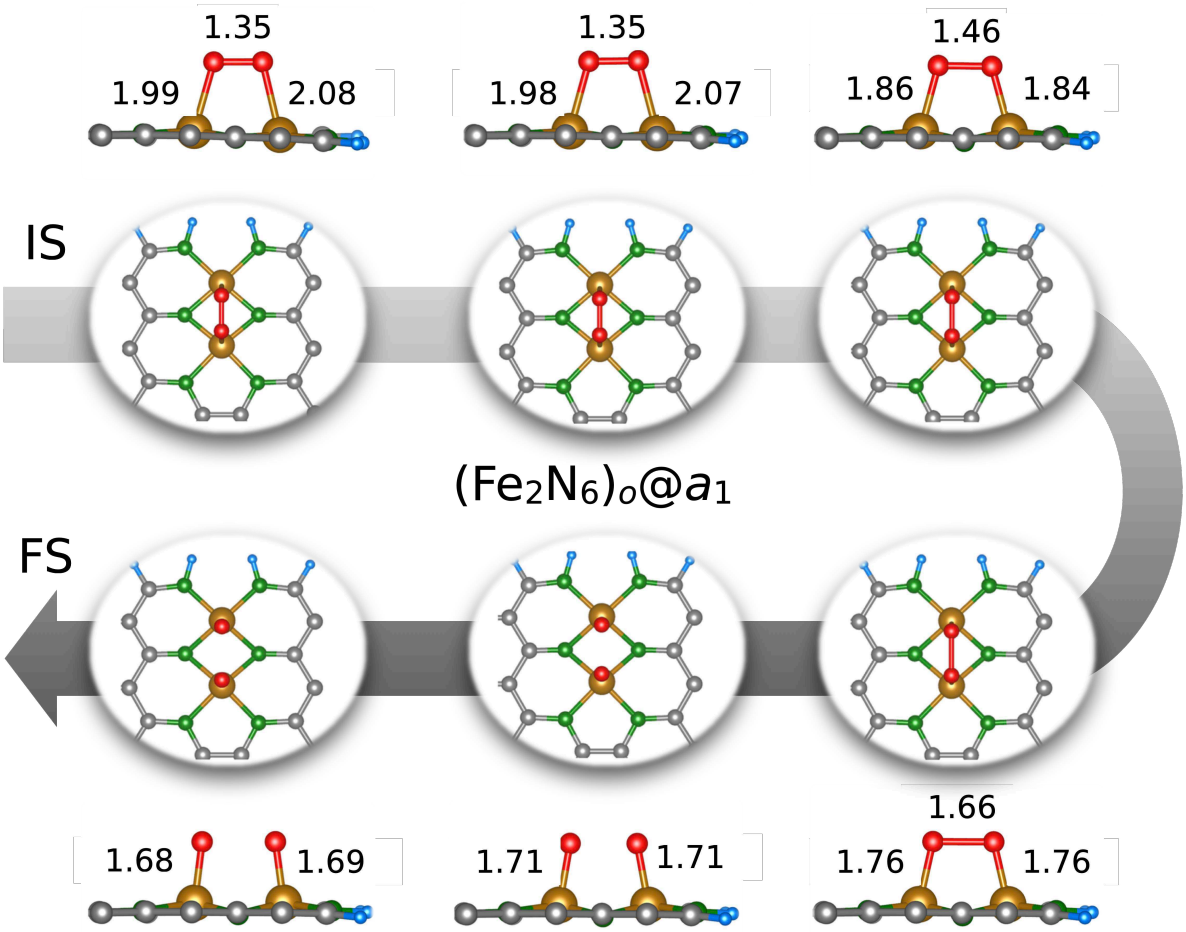

Figure S8: The O_2 dissociation on $(Fe_2N_6)_o@a_1$ calculated using NEB method. Grey, gold, red, green, and cyan spheres represent the C, Fe, O, N, and H atoms, respectively. Bond length is given in Å. IS and FS indicate the initial and final states, respectively.

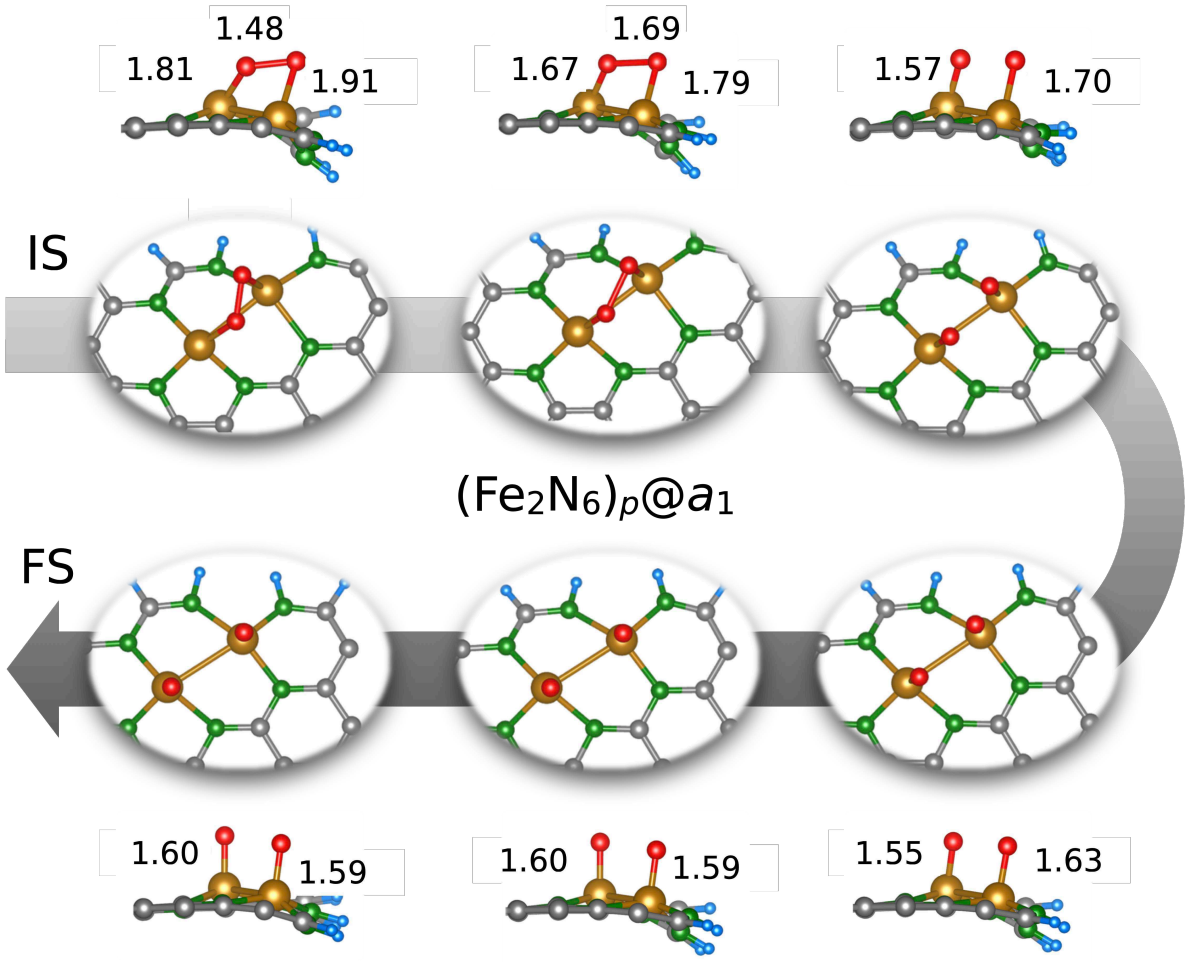

Figure S9: The O_2 dissociation on $(Fe_2N_6)_p@a_1$ calculated using NEB method. Grey, gold, red, green, and cyan spheres represent the C, Fe, O, N, and H atoms, respectively. Bond length is given in Å. IS and FS indicate the initial and final states, respectively.

7 Gibbs free energy profile

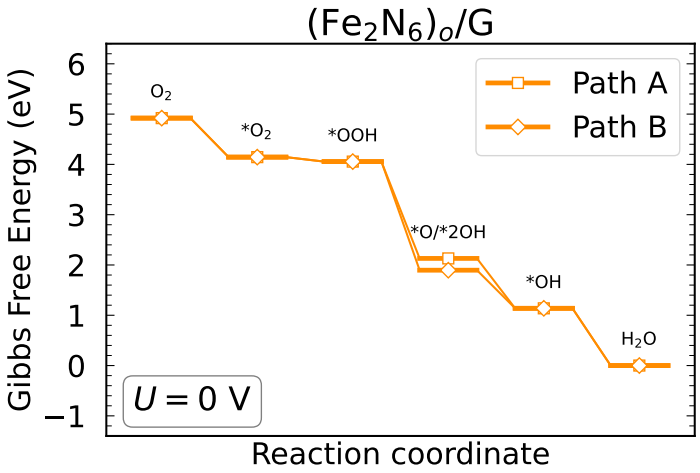

Figure S10: Gibbs free energy profile of $(Fe_2N_6)_o/G$ active site for the ORR associative mechanism at $U = 0$ V via both pathways A and B.

8 Logarithmic turnover frequency (ToF)

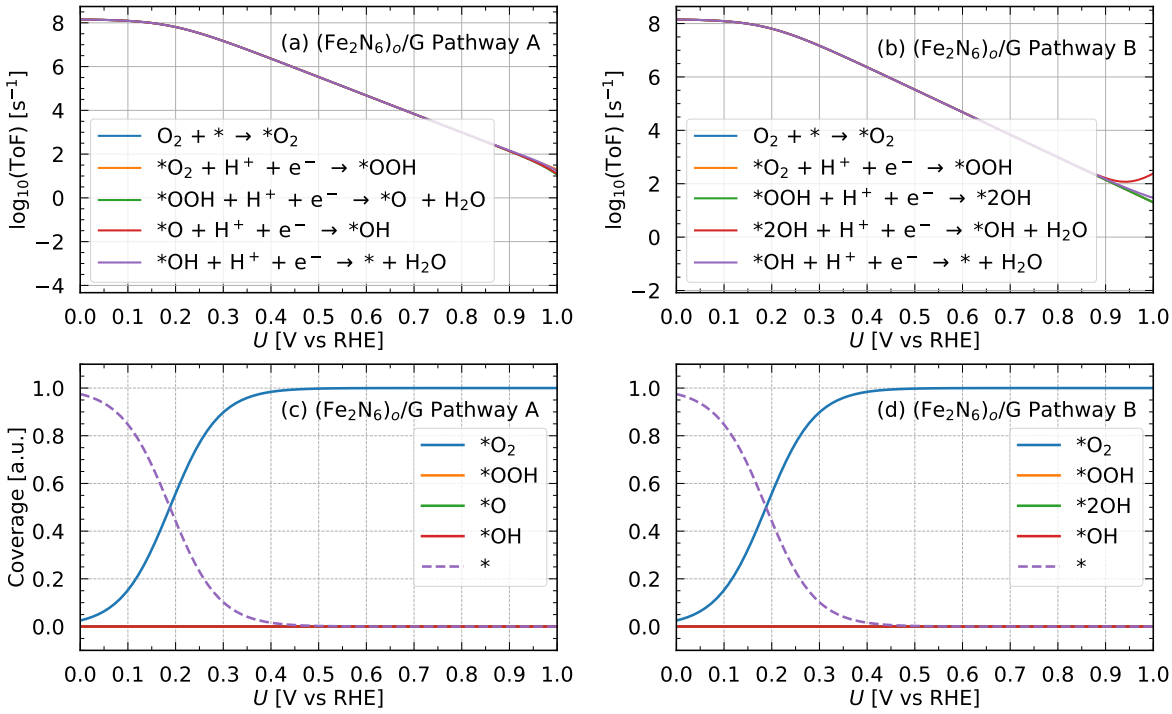

Figure S11: (a-b) Logarithmic turnover frequency (ToF) and (c-d) surface coverage as a function of electrode bias potential U in the ORR associative mechanism for $(Fe_2N_6)_o$/G via both pathways A and B.

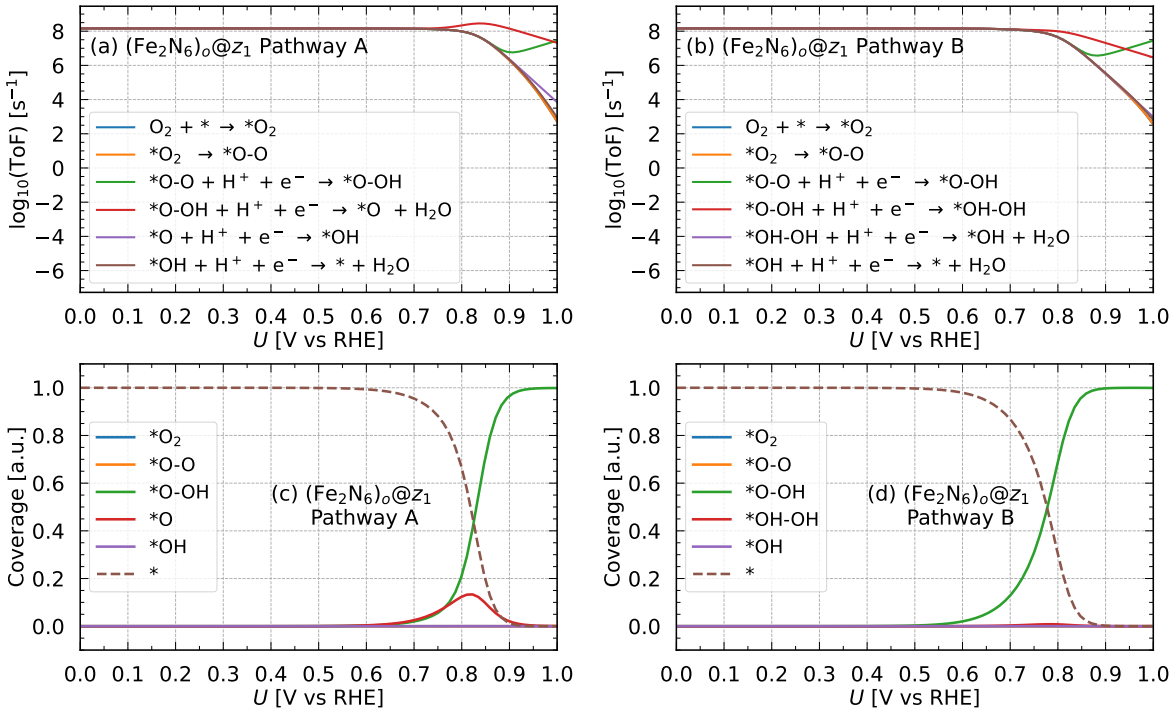

Figure S12: (a-b) Logarithmic turnover frequency (ToF) and (c-d) surface coverage as a function of electrode bias potential U in the ORR dissociative mechanism for $(Fe_2N_6)_o@z_1$ via both pathways A and B.

9 Surface coverage

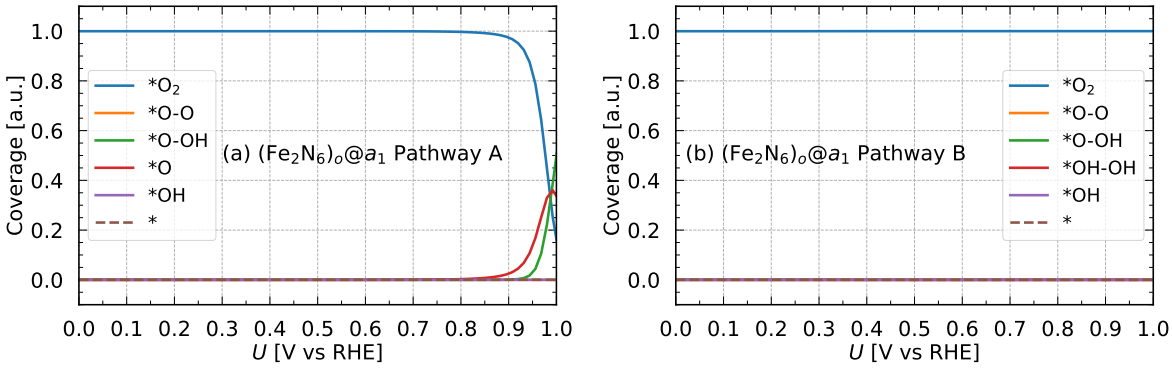

Figure S13: Surface coverage of $(Fe_2N_6)_o@a_1$ in ORR dissociative mechanism for both pathways (a) A and (b) B.